Journal of Cellular and Molecular Medicine
A JOURNAL OF TRANSLATIONAL MEDICINE

J. Cell. Mol. Med. Vol 15, No 12, 2011 pp. 2601-2613

# Nox2 and Nox4 mediate tumour necrosis factor-α-induced ventricular remodelling in mice

**K. T. Moe [a, *], N. O. Yin [a], T. M. Naylynn [a], K. Khairunnisa [a], M. A. Wutyi [a], Y. Gu [a], M. S. M. Atan [a], M. C. Wong [a], T. H. Koh [b], P. Wong [a, b]**

[a] *Research and Development Unit, National Heart Centre Singapore, Singapore*
[b] *Department of Cardiology, National Heart Centre Singapore, Singapore*

*Received: July 27, 2010; Accepted: January 7, 2011*

## Abstract

Reactive oxygen species (ROS) and pro-inflammatory cytokines are crucial in ventricular remodelling, such as inflammation-associated myocarditis. We previously reported that tumour necrosis factor-α (TNF-α)-induced ROS in human aortic smooth muscle cells is mediated by NADPH oxidase subunit Nox4. In this study, we investigated whether TNF-α-induced ventricular remodelling was mediated by Nox2 and/or Nox4. An intravenous injection of murine TNF-α was administered to a group of mice and saline injection was administered to controls. Echocardiography was performed on days 1, 7 and 28 post-injection. Ventricular tissue was used to determine gene and protein expression of Nox2, Nox4, ANP, interleukin (IL)-1β, IL-2, IL-6, TNF-α and to measure ROS. Nox2 and Nox4 siRNA were used to determine whether or not Nox2 and Nox4 mediated TNF-α-induced ROS and upregulation of IL-1β and IL-6 in adult human cardiomyocytes. Echocardiography showed a significant increase in left ventricular end-diastolic and left ventricular end-systolic diameters, and a significant decrease in the ejection fraction and fractional shortening in mice 7 and 28 days after TNF-α injection. These two groups of mice showed a significant increase in ventricular ROS, ANP, IL-1β, IL-2, IL-6 and TNF-α proteins. Nox2 and Nox4 mRNA and protein levels were also sequentially increased. ROS was significantly decreased by inhibitors of NADPH oxidase, but not by inhibitors of other ROS production systems. Nox2 and Nox4 siRNA significantly attenuated TNF-α-induced ROS and upregulation of IL-1β and IL-6 in cardiomyocytes. Our study highlights a novel TNF-α-induced chronic ventricular remodelling mechanism mediated by sequential regulation of Nox2 and Nox4 subunits.

**Keywords:** tumour necrosis factor-α • ventricular remodelling • NADPH oxidase • Nox2 • Nox4

## Introduction

Various pathologic stimuli have been shown to induce ventricular remodelling. These include myocardial infarction, chronic pressure overload (*e.g.* systemic arterial hypertension), chronic volume overload (*e.g.* valvular regurgitation), idiopathic dilated cardiomyopathy and inflammatory heart muscle disease (*e.g.* myocarditis) [1]. In addition, growing evidence has shown that endothelin, angiotensin II (AngII) and tumour necrosis factor-α (TNF-α) influence ventricular remodelling [2]. Elevated TNF-α levels have been reported to be directly related with functional heart failure [3] and TNF-α mRNA and protein have been shown to be uniformly expressed in failing human hearts [4]. TNF-α infusion in a rat model revealed a time-dependent increase in left ventricular end-diastolic dimension compared to time-matched controls [5]. Moreover, TNF-α transgenic mice, which generate cardiac-specific overexpression of TNF-α, showed four-chamber dilatation, myocyte hypertrophy, extracellular matrix (ECM) remodelling with fibrosis and premature death with a 6-month mortality of 25% [6]. However, there is no published evidence showing the TNF-α can induce chronic ventricular remodelling. Moreover, the molecular mechanism might that mediate TNF-α-induced cardiac remodelling is unclear.

Several mechanisms mediating cardiac and vascular remodelling have been suggested, including redox-sensitive signalling pathways. Despite the presence of many potential sources of reactive oxygen species (ROS), several studies have implicated

*Correspondence to: Dr. Kyaw Thu MOE, M.B.B.S., Ph.D.,
Research and Development Unit, National Heart Centre,
7 Hospital Drive, SingHealth Research Facilities,
Block A, #03-05, Singapore 169611,
Singapore.
Tel.: +(65) 63214282
Fax: +(65) 63213606
E-mail: moe.kyaw.thu@nhc.com.sg

doi: 10.1111/j.1582-4934.2011.01261.x

NADPH oxidase as a major source of ROS [7]. Many stimuli, including AngII, TNF-$\alpha$, platelet-derived growth factor, phorbol 12-myristate 13-acetate and transforming growth factor-$\beta_1$ (TGF-$\beta_1$) are able to activate NADPH oxidase, leading to cell proliferation, hypertrophy and inflammation of vascular smooth muscle cells, endothelial cells and cardiomyocytes [8]. We previously reported that TNF-$\alpha$-induced oxidative stress in human aortic smooth muscle cells was mediated by increased activity of NADPH oxidase *via* upregulation of Nox4, but not Nox2 [9]. Another study reported that AngII-induced hypertrophic changes in rat vascular smooth muscle cells were mediated by upregulation of Nox4 [10]. Moreover, a recent study reported that human pulmonary artery smooth muscle cell proliferation induced by TGF-$\beta_1$ was mediated by upregulation of Nox4 [11], suggesting that the Nox4 gene plays a crucial role in vascular cell remodelling.

However, the role of Nox subunits in cardiac remodelling is controversial. A previous study revealed that AngII increased NADPH oxidase activity with hypertrophy of cardiomyocytes in wild-type mice, but not in Nox2$^{-/-}$ mice, suggesting a crucial role of Nox2 in AngII-induced cardiac hypertrophy [12]. Another study demonstrated that aortic constriction increased NADPH oxidase activity with upregulation of both Nox4 mRNA and protein and left ventricular hypertrophy (LVH) in both Nox2$^{-/-}$ and wild-type mice, suggesting a distinct role of Nox4 in response to pressure overload [13]. Interestingly, a recent study of myocardial infarction induced by coronary artery ligation did not show any significant differences of cardiac remodelling between wild-type and Nox2$^{-/-}$ mice, suggesting a compensatory mechanism that produces cardiac oxidative stress in Nox2$^{-/-}$ mice [14].

In this study, we hypothesized that Nox2 and Nox4 play a crucial role, mediating TNF-$\alpha$-induced ventricular remodelling. Murine TNF-$\alpha$ was injected intravenously into the tail veins of adult Swiss Albino mice and molecular changes of ventricular remodelling examined at different time points. Our study showed that Nox2 and Nox4 sequentially regulate TNF-$\alpha$-induced ventricular remodelling in mice, mediate TNF-$\alpha$-induced ROS and upregulation of IL-1$\beta$ and IL-6 in human adult cardiomyocytes.

# Materials and methods

## Animals and experimental design

Male Swiss Albino mice (7–8 weeks old; 25–30 g in weight) were used for the study. A single dose of murine TNF-$\alpha$ (R&D Systems, Minneapolis, MN, USA) was administered *via* intravenous injection at 8 $\mu$g/kg body weight to a group of mice ($n = 15$). An equivalent volume of saline was administered to control mice ($n = 13$) [15]. Echocardiography was performed on 1, 7 and 28 days post-injection ($n = 4$ or 5 in each group). Standard laboratory chow and water were available *ad libitum*. After echocardiographic assessments, mice were sacrificed, hearts removed and stored in liquid nitrogen. Heart and body weights were recorded at all three time points. All protocols and experimental procedures were performed in accordance with the Guidelines for the Care and Use of Research Animals and were approved by the SingHealth Institutional Animal Care and Use Committee.

## Cardiomyocytes culture, siRNA transfection and TNF-$\alpha$ treatment

Adult human cardiomyocytes were obtained from PromoCell GmbH (Heidelberg, Germany) and maintained in myocyte growth medium according to the manufacturer's instructions. Cells were used between passage 3 and 6, and at 85–90% confluence.

All small interfering RNA (siRNA) sequences and transfection reagents were purchased from Ambion (Austin, TX, USA). Silencer® Pre-designed siRNA (Nox2 siRNA, ID 3915 and Nox4 siRNA, ID 24766) were used to knock down Nox2 and Nox4 genes in human adult cardiomyocytes, respectively. siRNA sequences were transfected with siPORT Amine (AM4502) according to the manufacturer's instruction. The Silencer® Negative Control siRNA (ID 4618G) was used as a negative control. Cells were sub-cultured in six-well plates and transfection was performed within 24 hrs, followed by treatment with TNF-$\alpha$ (20 ng/ml) for 6 hrs at 37°C, according to previously described methods [9].

## Echocardiography

Echocardiography was performed using GE Vivid 7 with a linear 13 MHz probe (GE VingMed, Horten, Norway) under 1.0–1.5% isoflurane and spontaneous respiration [16]. Two-dimensional guided M-mode echocardiography of the left ventricular at the papillary muscle level was obtained from the short-axis view. Measurements were performed using an offline analysis system (GE EchoPac). The parameters were measured from three consecutive cardiac cycles on the M-mode tracings. Cardiac function was assessed by left ventricular end diastolic (LVEDD) and systolic diameters (LVESD), ejection fraction (EF) and fractional shortening (FS).

## Histology

Cryostat sections (5 $\mu$m) were prepared to investigate ROS and myocyte hypertrophy in the ventricles of the mice. All measurements were performed on three different randomly chosen fields/sections on at least three serial sections for each animal following the procedures previously described [17, 18].

Dihyro-ethidium (DHE; Molecular Probes, Invitrogen, Eugene, OR, USA) was used to evaluate the presence ROS following methods previously described [17]. In the presence of ROS, DHE is oxidized to ethidium bromide, which binds DNA. The fluorescence reaction was carried out by incubating heart sections with DHE ($2 \times 10^{-6}$ mol/L) for 30 min at 37°C. Fluorescence intensity in each heart section was normalized with fluorescence intensity detected in the respective control sections and expressed as arbitrary fluorescence units (AFU).

MitoSOX Red (Molecular Probes) was used to examine the presence of mitochondrial ROS following the methods previously described [19]. MitoSOX Red is selectively targeted to the mitochondria. Once in the mitochondria, MitoSOX Red reagent is oxidized by superoxide and exhibits red fluorescence. The fluorescence reaction was carried out by incubating the heart sections with MitoSOX Red (5 $\mu$M) for 10 min at

37°C. Fluorescence intensity in each heart section was normalized with fluorescence intensity detected in the respective control sections and expressed as AFU.

A single cardiomyocyte was measured with images captured with haematoxylin and eosin-stained sections of mouse ventricular tissue. The outline of 30–50 myocytes was traced in each section and the cross-sectional area was obtained in a blinded fashion with AxioVs40 V4.7 software (Zeiss, Germany) in a Zeiss Axiovert 200M microscope following the procedures previously described [20].

## Immunohistochemistry

Alpha-smooth muscle actin (α-SMA) expression in the ventricles was determined following the methods previously described with slight modification [14, 21]. Cryostat sections were fixed in ice-cold acetone for 15 min, and air-dried. Endogenous peroxidase activity was blocked by incubating the sections with 1% $H_2O_2$ for 20 min. After incubating the sections with M.O.M. mouse Ig blocking reagent using Mouse on Mouse kit (Vector Laboratories, Burlingame, CA, USA) for 60 min, the sections were incubated with mouse anti-α-SMA (Santa Cruz Biotechnology Inc.) for 30 min. Secondary antibody was diluted in mouse diluent and the sections were incubated with secondary antibody for 15 min. The signal was detected by VECTASTAIN ABC reagent following manufacturer's instruction (Vector Laboratories). The images were analysed using Image Pro Plus software 6.0 (Media Cybernetics, Silver Spring, ML, USA).

## Cytokine assays

The concentrations of IL-1β, IL-2, IL-6 and TNF-α were analysed in ventricular homogenates following procedures previously described [22]. Dissected tissues were homogenized (Ultra Turrax T8, Tamro, Sweden) in homogenization buffer containing PBS [10 mM sodium phosphate buffer (pH 7.3) and 0.15 M NaCl] and Halt™ Protease Inhibitor Cocktail (Pierce, Rockford, IL, USA) following the manufacturer's instructions. The homogenized solution was centrifuged for 10 min at 18,000 rpm, and the supernatant was separated into aliquots and frozen at −80°C until analysis. The concentrations of IL-1β, IL-2, IL-6 and TNF-α were determined using Bioplex Multiplex Suspension Array System kits, according to the manufacturer's instructions (Bio-Rad Laboratories, Hercules, CA, USA), and subsequently analysed with Bioplex Manager 3.0 software (Bio-Rad Laboratories). The homogenization buffer was used to generate the standard curve as a background to be subtracted from the standards as well as the samples and to dilute the samples 1:2 before analysis. The protein values are expressed as picograms per mg of ventricular protein.

## Trolox equivalent antioxidant capacity (TEAC) assay

TEAC, an indicator of total antioxidant capacity of plasma was measured following the method previously described [23]. The assay relies on the ability of antioxidants in the plasma to inhibit the oxidation of 2,2′-Azino-di-[3-ethylbenzthiazoline sulphonate] (ABTS). The antioxidants in the sample cause the suppression of the absorbance at 750 nm to a degree, which is proportional to their concentration. The capacity of antioxidants in the sample to prevent ABTS oxidation is compared with that of Trolox, a water-soluble tocopherol analogue, and is quantified as millimolar Trolox equivalents.

## Determination of antioxidant activity in the ventricular tissue

Glutathione assay and superoxide dismutase (SOD) assay were performed to determine the antioxidant status of ventricular tissues. Approximately 0.1 g of tissue from each sample was used for each experiment according to the manufacturer's instructions.

The glutathione assay was performed to determine the total glutathione GSH (GSH and GS-SG) using a Glutathione Assay Kit (Cayman Chemical Co., Ann Arbor, MI, USA) following the methods previously described [24]. The kit uses an enzymatic recycling method using glutathione reductase to quantify glutathione (GSH). The sulfhydryl group of GSH reacts with 5,5′-dithio-bis-2-nitrobenzoic acid (DTNB) and produces a yellow coloured 5′-thio-2-nitrobenzoic acid (TNB). The mixed disulfide GSTNB is reduced by glutathione reductase to recycle the GSH and produce more TNB. Measurement of the absorbance of TNB at 405 nm provides an accurate estimation of GSH in the ventricular tissue.

Ventricular SOD activity was measured using a Superoxide Dismutase Assay Kit (Cayman Chemical Co.) following the methods previously described [25, 26]. The superoxide radical agents formed by the interaction of xanthine oxidase with hypoxanthine were detected by tetrazolium. One unit of SOD detected is equivalent to the amount of enzyme needed to exhibit 50% dismutase of superoxide radical.

## NADPH oxidase activity assay

NADPH-dependent ROS production was measured in ventricular homogenates using 5 (and 6)-chloromethyl-2′, 7′-dichlorodihydrofluorescein diacetate-acetyl ester (CM-$H_2$DCFDA; Molecular Probes) in 100 μg protein following the procedures previously described [13, 27]. The protein and probe were added to Falcon 96-well black microplates (Becton Dickinson, Franklin Lakes, NJ, USA) in triplicate. Probe-free cell sonicate was used for blanks. Ethidium fluorescence was measured in a 1420 Wallac Victor3 multilabel counter (Perkin-Elmer Life Sciences, Cambridge, UK) using excitation and emission wavelengths of 490 and 605 nm, respectively. All measurements were performed in triplicate. Some experiments were performed in the presence of the NADPH oxidase inhibitor, diphenyleneiodonium (DPI; $10^{-5}$ M) and apocynin (1 mM), the xanthine oxidase inhibitor, allopurinol (1 mM), SOD (60 units/ml), the NO synthase inhibitor, L-NAME (100 μM) or mitochondrial respiration inhibitor, rotenone (1 μM) [9].

## RNA extraction and real-time RT-PCR

Total RNA was extracted from the ventricular tissues and cultured human adult cardiomyocytes using TRIzol reagent (Invitrogen, Carlsbad, CA, USA) following the previously described methods [28], and quantified on a NanoDrop 1000 Spectrophotometer (Thermo Scientific Inc., Wilmington, DE, USA). First strand cDNA synthesis was performed with 700 ng of total RNA using the SuperScriptII first-strand synthesis system for RT-PCR (Invitrogen). Three microlitres of first strand reaction was used for each 25 μl PCR reaction using TaqMan® Universal PCR Master Mix (Applied

**Table 1** Gene symbol, assay ID and RefSeq for RT-PCR

| | Gene Symbol | Assay ID | RefSeq |
|---|---|---|---|
| Mouse | Nox2 | Mm00627011_m1 | NM_007807.4 |
| | Nox4 | Mm00479246_m1 | NM_015760.4 |
| | ANP | Mm01255747_g1 | NM_008725.2 |
| | GAPDH | Mm03302249_g1 | NM_008084.2 |
| Human | Nox2 | Hs00166163_m1 | NM_000397.3 |
| | Nox4 | Hs00418356_m1 | NM_016931.3 |
| | IL-1β | Hs00174097_m1 | NM_000576.2 |
| | IL-6 | Hs00174131_m1 | NM_000600.2 |
| | GAPDH | Hs99999905_m1 | NM_002046.3 |

Biosystems International, Foster City, CA, USA), together with 2.5 μl of Taqman® Gene Expression Assays primers. Real-time quantitative PCR analysis was conducted to examine the gene expressions of mouse (Nox2, Nox4, ANP and GAPDH) and human (Nox2, Nox4, IL-1β, IL-6 and GAPDH) genes using an Applied Biosystems 7300 Real-Time PCR System (Applied Biosystems International). The assay ID and RefSeq of each gene are listed in Table 1. After an initial incubation step for 2 min at 50°C and denaturation for 10 min at 95°C, PCR was performed using 40 cycles (95°C for 15 s and 60°C for 60 s). Equal amounts of input RNA were used for all RT-PCR reactions, reactions were performed in duplicate, and GAPDH was used as an internal control. Total RNA with no reverse transcription (-RT) was used as a negative control. Differential gene expression analysis was calculated using the Comparative (ΔΔCT) method, as described previously [28].

## Immunoblotting

Ventricular homogenates were prepared and the concentration of protein was quantified with a NanoDrop 1000 Spectrophotometer. For immunoblotting, the same amount of protein was loaded in each lane of the SDS-PAGE gels and afterwards transferred to polyvinylidenefluoride (PVDF) membranes. Mouse Nox2, Nox4 and ANP proteins were examined using purified anti-gp91phox (BD Biosciences, San Diego, CA, USA), anti-Nox4 antibody (Novus Biologicals, Littleton, CO, USA) and anti-ANP (Santa Cruz Biotechnology Inc.), following the procedures previously described [9]. After incubation with HRP-conjugated secondary antibody, proteins were detected by SuperSignal® West Pico Chemiluminescent Substrate (Pierce). Each membrane was re-probed with anti-GAPDH (Santa Cruz Biotechnology Inc.) after removing with Restore™ Western Blot Stripping Buffer (Pierce). The signals were analysed using AlphaEase® FC software and FluorChem HD2 (Alpha Innotech Corp., San Leandro, CA, USA).

## Statistical analysis

All data are expressed as the mean ± S.D. or S.E. In experiments in which more than two groups are compared each other with ANOVA, followed by Fischer's least significance *post hoc* test or Student's unpaired t-tests. Differences were considered significant when $P$ values were $<0.05$.

# Results

## Increased oxidative stress in ventricular tissue of TNF-α-treated mice is mediated by NADPH oxidase

To detect ROS in the *ex vivo* ventricular tissues of TNF-α-injected and control mice, DHE staining was performed. No significant difference in fluorescent intensity was observed among day-1 TNF-α-injected and control mice (Fig. 1A and B). However, the fluorescent intensities of mice injected with TNF-α 7 and 28 days previously were significantly higher than control mice. Mitochondrial ROS in the *ex vivo* ventricular tissues of TNF-α-injected and control mice showed slight fluorescence intensity (Fig. 1C). However, there was no significant difference between TNF-α injected and control mice at all three time points (Fig. 1D). The ROS in the ventricular homogenates was assessed by CM-$H_2$DCFDA fluorescence assay. Mice injected with TNF-α 7 and 28 days previously showed a significant increase in fluorescence compared to the controls, but not in the mice injected 1 day previously (Fig. 1E). The enzymatic sources of the ROS were examined using specific inhibitors in the fluorescence assay. ROS production was significantly reduced with SOD and abolished by NADPH oxidase inhibitors, DPI and apocynin. However, allopurinol, L-NAME and rotenone had no effect on TNF-α-induced ROS in the ventricles (Fig. 1F).

The total antioxidant capacity of plasma (TEAC) assay showed that there was no significant difference in TEAC between TNF-α injected mice and control mice at all three time points. However, a slight increase in TEAC was observed in mice injected with TNF-α 7 and 28 days previously compared to control mice (Fig. 1G). Similar finding was observed in total GSH levels in the ventricles of TNF-α-injected and control mice. Total GSH levels were slightly higher in those of TNF-α-injected mice at all three time points compared to controls (Fig. 1H). However, ventricular SOD levels show no difference among TNF-α-injected and control mice (Fig. 1I).

## Nox2 and Nox4 subunits are up-regulated in the ventricles of TNF-α-treated mice

Ventricular homogenates from both TNF-α-injected and control mice were used to determine Nox2 and Nox4 mRNA levels by real-time PCR and protein levels by immunoblotting. Analysis of Nox2 mRNA revealed a significant increase in mice injected with TNF-α 1 day previously (1.6-fold) compared to controls (Fig. 2A). However, no significant difference was observed between Nox2 mRNA levels of mice injected with TNF-α 7 and 28 days previously and control mice.

Analysis of Nox4 mRNA showed that it was different from the Nox2 mRNA expression profile. Nox4 mRNA levels were similar in mice injected with TNF-α 1 day previously and control mice (Fig. 2B); however, mice injected with TNF-α 7 and 28 days previously were significantly increased (3- and 1.5-fold, respectively) compared to the control mice.

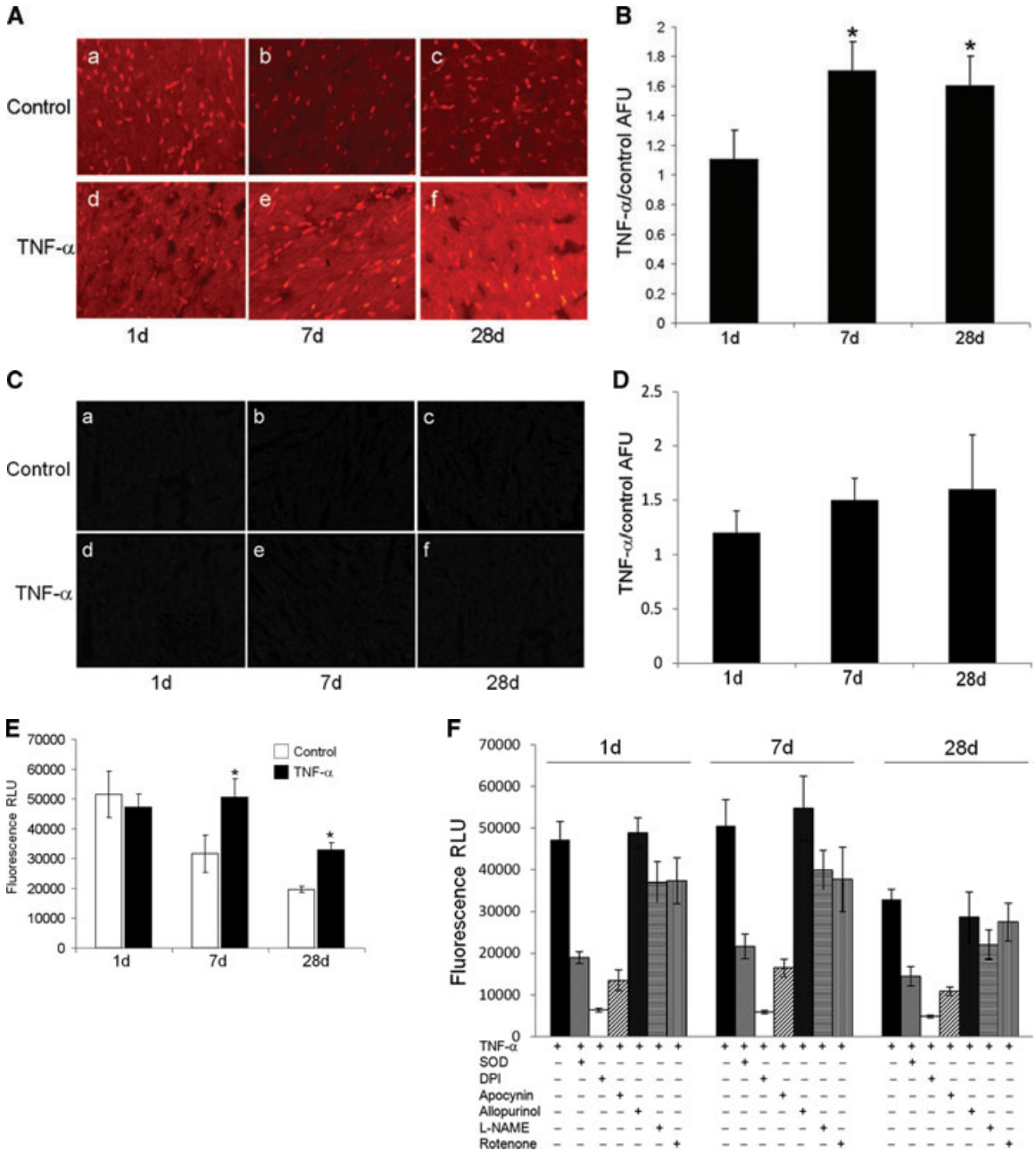


**Fig. 1** Increased ROS production in ventricles of TNF-α-injected mice. The ROS in the ventricular tissues were detected by incubating the cryostat sections with DHE ($2 \times 10^{-6}$ mol/L) for 30 min at 37°C. Representative of DHE staining of ventricular tissues were shown (**A**). Magnification = 40×. Fluorescence intensities in the sections of TNFα-injected mice were normalized with controls. Data were expressed as arbitrary fluorescence units (AFU) ± S.D. (**B**). Mitochondrial ROS in the ventricular tissues were detected by incubating the sections with MitoSOX Red (5 μM) for 10 min at 37°C. Representative of MitoSOX Red staining of ventricular tissues were shown (**C**) and normalized fluorescence intensities were shown (**D**). ROS in the ventricular homogenates was determined with CM-$H_2$DCFDA. The fluorescence intensities of ventricular homogenates of TNF-α-injected and control mice were shown (**E**). The source of ROS production in the ventricles of TNF-α-injected mice was determined using different inhibitors. NADPH oxidase inhibitors (DPI and apocynin) significantly decreased ROS (**F**). Data were expressed as relative light unit (RLU) ± S.D. SOD, superoxide dismutase; DPI, diphenyleneiodonium; L-NAME, $N^G$-nitro-L-arginine methyl ester. Trolox equivalent antioxidant capacity (TEAC) assay was performed to detect capacity of antioxidants in the plasma and quantified as millimolar Trolox equivalent (**G**). Glutathione assay and superoxide dismutase assay were performed to determine the total GSH (**H**) and SOD levels (**I**) in the ventricles of TNF-α-injected and control mice respectively. $^*P < 0.05$.

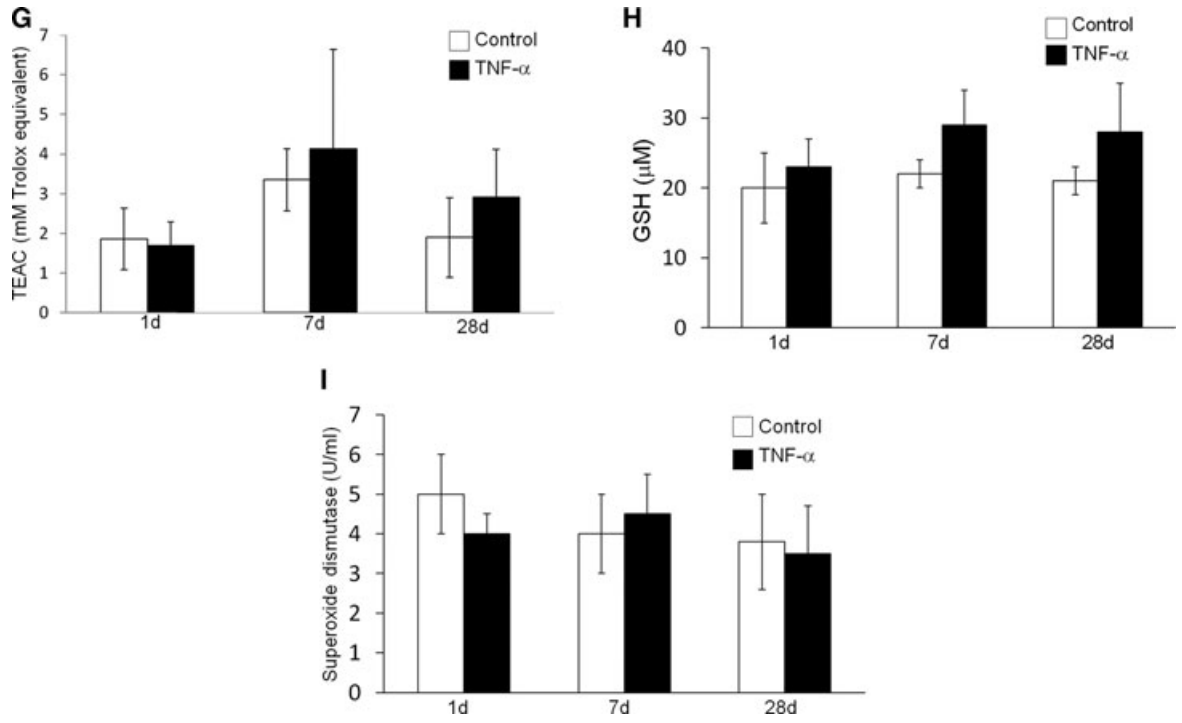


**Fig. 1** Continued

Both Nox2 and Nox4 proteins were detected in all samples with the molecular weights identified in the manufacturer's protocol. Nox2 and Nox4 protein expression were similar to the mRNA profile. The Nox2 protein level of mice injected with TNF-α 1 day previously was significantly increased compared to controls (Fig. 2C and D), whereas the protein levels of mice injected with TNF-α 7 and 28 days previously and control mice showed no significant differences. However, Nox4 protein expression of mice injected with TNF-α 7 and 28 days previously was significantly increased by 100% compared to controls (Fig. 2C and E), whereas mice injected with TNF-α 1 day previously and control mice were similar.

## Ventricular tissues of TNF-α-treated mice are inflamed until 28 days post-injection

We measured IL-1β, IL-2, IL-6 and TNF-α protein concentrations in ventricular tissue lysates. All four cytokines in mice injected with TNF-α were significantly elevated compared to controls until 28 days post-injection (Fig. 3). IL-1β concentrations of TNF-α-injected mice were significantly elevated at 7 days post-injection compared to controls and more than 170% increased compared to TNF-α-injected mice 1 day post-injection (Fig. 3A). IL-1β remained elevated until 28 days post-injection and was significantly higher than controls. Progressive elevation of IL-2 and IL-6 concentrations were observed in mice injected with TNF-α 7 and 28 days previously, whereas TNF-α-injected mice 1 day post-injection showed the same level compared to controls (Fig. 3B and C). TNF-α protein concentrations in the ventricular tissue of TNF-α-injected mice were significantly increased at all three time points (Fig. 3D). These elevated levels of pro-inflammatory cytokines showed that ventricles of TNF-α injected mice are inflamed.

## Ventricular tissues of TNF-α-treated mice underwent hypertrophy until 28 days post-injection

TNF-α injection into the mice resulted in hypertrophy of cardiomyocytes 7 and 28 days post-injection. The myocyte cross-sectional area showed a significant increase in mice injected with TNF-α 7 and 28 days previously compared to controls, while there was no significant change in myocyte area between day-1 treated and control mice (Fig. 4A). The heart and body weight ratio (HW/BW) also increased in mice injected with TNF-α 7 and 28 days previously (Fig. 4B). However, the significant difference was observed only mice 28 days post-injection.

There was a significant increase in ANP gene expression at all three time points. Mice injected with TNF-α 1, 7 and 28 days previously showed a 1.5-, 9- and 4-fold increase, respectively, compared to controls (Fig. 4C). These data were consistent with immunoblotting analysis of ANP, which revealed a significant increase in ANP protein levels in TNF-α injected mice at all three

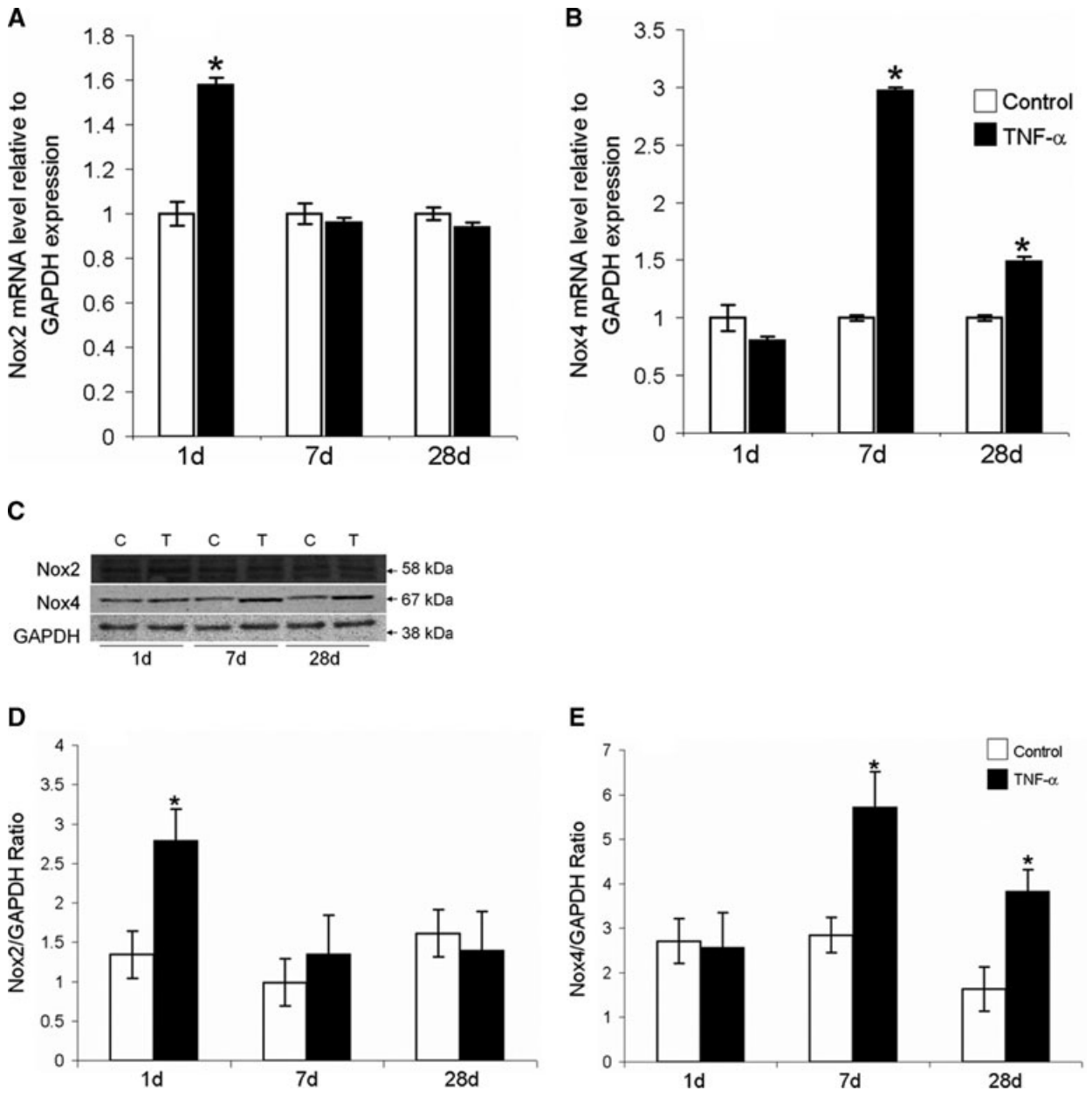


**Fig. 2** Upregulation of Nox2 and Nox4 mRNA and protein in ventricles of TNF-α-injected mice. Total RNA was extracted from the ventricular tissues of TNF-α-injected and control mice and Nox2 and Nox4 mRNA levels were examined using real-time PCR. Nox2 (**A**) and Nox4 mRNA levels (**B**) were shown. Nox2 and Nox4 protein levels were determined by immunoblotting. A representative of Nox2 and Nox4 proteins were shown (**C**). Densitometric analysis of Nox2 (**D**) and Nox4 protein (**E**) normalized with GAPDH were shown. C, control; T, TNF-α-injected mice. $^*P < 0.05$.

time points compared to controls (Fig. 4D). α-SMA expressions detected by immunohistochemistry showed that the expression was increased in mice injected with TNF-α 7 and 28 days previously (Fig. 5). However, the significant difference in α-SMA expression level was observed in the mice 28 days post-injection.

## Ventricular dysfunction in TNF-α-treated mice

Left ventricular cardiac function of all mice was evaluated *in vivo* with echocardiography (GE Vivid 7 with a linear 13 MHz probe). LVEDD was significantly increased 28 days post-injection,

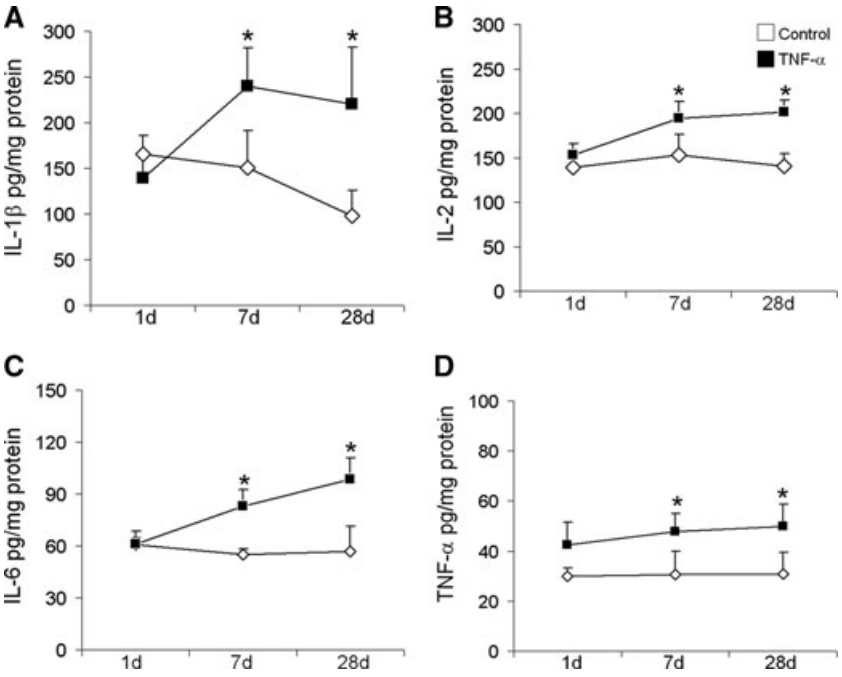


**Fig. 3** Elevated pro-inflammatory cytokine concentrations in the ventricles of TNF-α-injected mice. The ventricular homogenates were used to determine the pro-inflammatory cytokine concentrations using Bioplex Multiplex Suspension Array System kits. The concentrations of IL-1β (**A**), IL-2 (**B**), IL-6 (**C**) and TNF-α (**D**) were shown. Data are expressed as pg/mg of ventricular protein ± S.D. $^*P < 0.05$.

whereas LVESD was significantly increased in mice injected with TNF-α 7 and 28 days post-injection compared to controls (Table 2). A significant decrease in the LVEF and FS was noted in mice injected with TNF-α 7 and 28 days previously compared to controls.

### TNF-α-induced IL-1β and IL-6 upregulation, and ROS production in adult human cardiomyotes is mediated by Nox2 and Nox4

Nox2 siRNA and Nox4 siRNA significantly decreased Nox2 and Nox4 mRNA levels by 45% and 80%, respectively, in adult human cardiomyocytes (Fig. 6A and B). However, Nox2 and Nox4 siRNA showed no changes in Nox4 and Nox2 mRNA, respectively (data not shown). The role of Nox2 and Nox4 in TNF-α-induced pro-inflammatory cytokine IL-1β and IL-6 expression, and ROS production was determined after knocking down Nox2 and Nox4. Nox2 siRNA significantly decreased TNF-α-induced upregulation of IL-1β by 50% and IL-6 by 25% (Fig. 6C and D). Nox4 siRNA also significantly decreased TNF-α-induced upregulation of IL-1β by 45% and IL-6 by 30%. Nox2 and Nox4 siRNA had no effect on IL-1β and IL-6 expression without TNF-α treatment. Control siRNA had no effect on TNF-α-induced upregulation of IL-1β and IL-6 (data not shown). Finally, Nox2 and Nox4 siRNA significantly decreased TNF-α-induced ROS production by 40% and 50%, respectively (Fig. 6E).

## Discussion

The major finding of this study was that the pro-inflammatory cytokine TNF-α-induced ventricular remodelling in mice up to 4 weeks after receiving a single dose, and this effect appeared to be regulated by NADPH oxidase-mediated ROS and upregulation of Nox2 and Nox4 subunits. Furthermore, Nox2 and Nox4 appeared to sequentially regulate the development of ventricular remodelling in mice (Nox2 for the short-term and Nox4 for the long-term development of ventricular remodelling). Another significant finding was TNF-α-induced elevation of other pro-inflammatory cytokines (IL-1β, IL-2 and IL-6) and TNF-α in the ventricles. Moreover, we confirmed that TNF-α-induced ROS production and upregulation of IL-1β and IL-6 in human adult cardiomyocytes was mediated by the NADPH oxidase subunits Nox2 and Nox4.

Our findings are consistent with and extend published reports. Sun *et al.* [29] reported that excessive activation of TNF-α in the myocardium contributed to the development of chronic left ventricular dysfunction by inducing a local inflammatory response. Levine *et al.* [30] demonstrated elevated levels of TNF-α in patients with left ventricular dysfunction in the absence of clinical symptoms of heart failure, as well as patients with end-stage heart failure. Interestingly, Bozkurt *et al.* [5] reported that continuous infusion of recombinant human TNF-α into adult Sprague–Dawley rats led to time-dependent depression in left ventricular function, cardiac myocyte shortening and left ventricular dilatation that

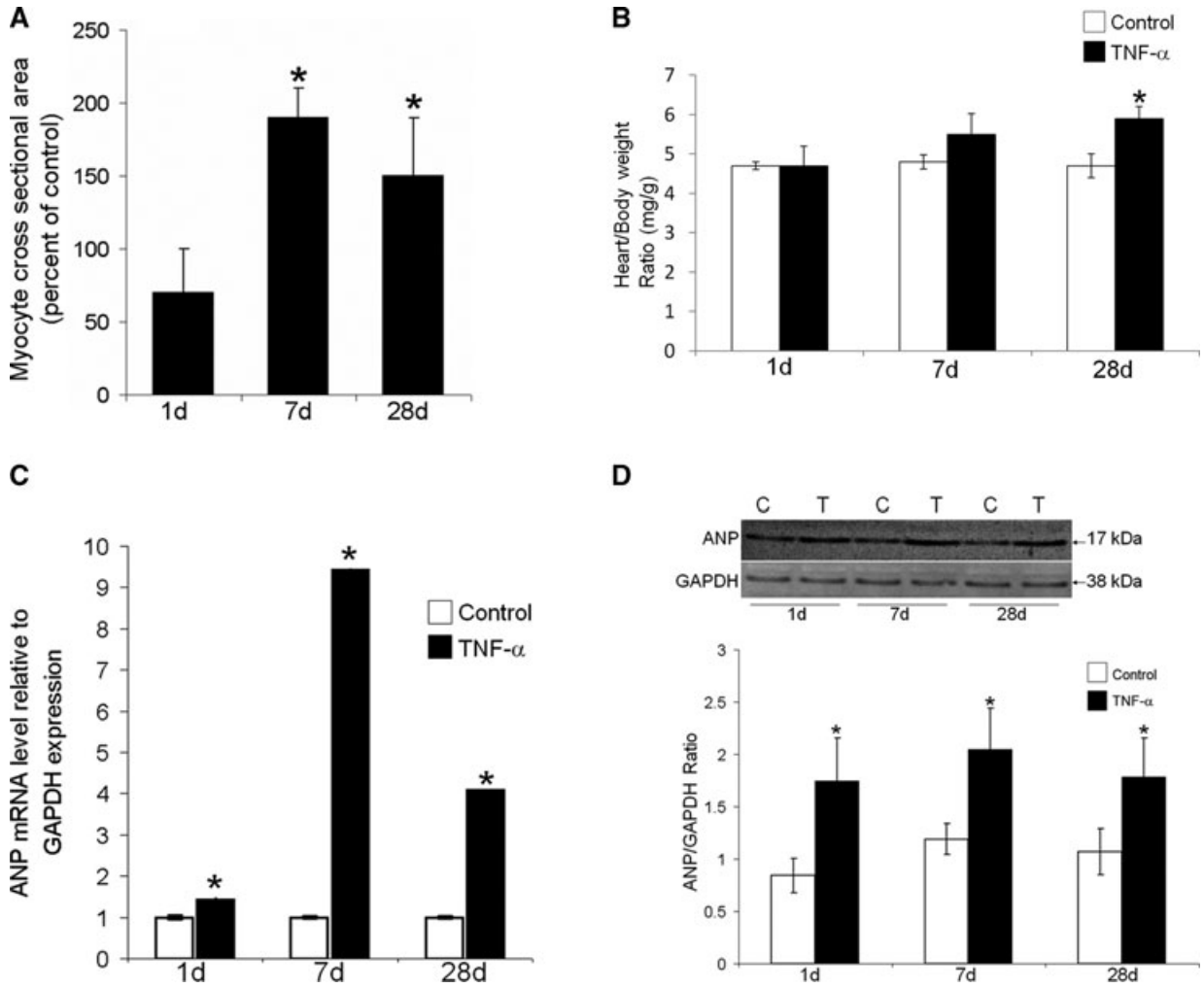


**Fig. 4** TNF-α-induced ventricular hypertrophy. Cryostat sections were prepared and stained with haematoxylin and eosin. Each cardiomyocytes was measured and outline of 30–50 cardiomyocytes was traced in each field. The cross-sectional area was obtained in a blinded fashion with AxioVs40 V4.7 software. Mean values of cardiomyocytes cross-sectional areas of TNF-α-injected mice were normalized with those of controls. Cardiomyocyte cross-sectional area was presented as a percentage of control ± S.D. (**A**). Heart and body weight ratios were presented in mg/g ± S.D. (**B**). Total RNA was extracted from the ventricles and ANP mRNA levels were examined using real-time PCR. ANP mRNA level relative to GAPDH was shown (**C**). Data were expressed as fold ± SD. Ventricular homogenates were examined for ANP protein level by immunoblotting. A representative of ANP proteins was shown (**D**). C, control; T, TNF-α-injected mice. Densitometric analysis of ANP protein (below) was normalized with GAPDH. $*P < 0.05$.

were reversible by removal of the TNF-α infusion pump. However, the authors cautioned that formation of rat autoantibodies against human TNF-α could be responsible for the reversal of cardiac remodelling. Contrary to their finding, administration of murine TNF-α could induce chronic ventricular remodelling in mice in this study. This discrepancy in the findings may arise from the use of a specific ligand to bind its receptor, which led to greater intermolecular force and affinity [31]. In addition, arterial dilatation and venular constriction in the retina as well as proliferation of smooth muscle cells in the abdominal aorta were observed in these mice (data not shown). This suggested that elevated levels of TNF-α triggered intracellular signalling cascades that led to inflammatory changes in the vessels.

TNF-α has been reported to have a biphasic (immediate and delayed) nature of myocardial depression [32]. The early phase of TNF-α-induced myocardial depression occurs within minutes after TNF-α administration due to sphingosine production in the myocardium that leads to myocardial dysfunction and calcium dyshomeostasis in cardiomyocytes [33]. The delayed phase of TNF-α-induced functional depression occurs several hours after

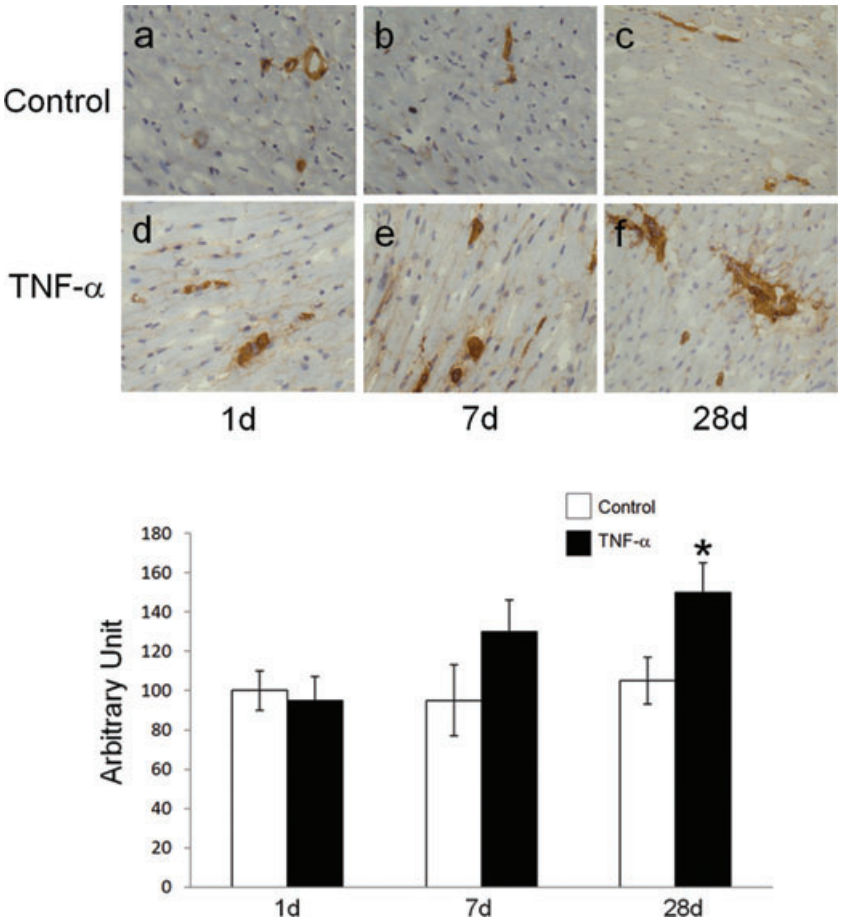


**Fig. 5** Increased α-SMA expression in the ventricular tissues of TNF-α-injected mice. α-SMA expression was examined by immunohistochemistry using mouse anti-α-SMA antibody. The images were analysed using Image Pro Plus software 6.0 and the values were presented with arbitrary units ± S.D. $*P < 0.05$.

**Table 2** Echocardiographic measurements of TNF-α-injected and control mice

| | 1d | | 7d | | 28d | |
|---|---|---|---|---|---|---|
| | **Control** | **TNF-α** | **Control** | **TNF-α** | **Control** | **TNF-α** |
| LVEDD (mm) | 4.39 ± 0.08 | 4.32 ± 0.07 | 4.45 ± 0.04 | 4.34 ± 0.03 | 4.33 ± 0.05 | 4.59 ± 0.06* |
| LVESD (mm) | 2.85 ± 0.05 | 2.62 ± 0.05 | 2.65 ± 0.02 | 2.83 ± 0.04* | 2.70 ± 0.03 | 3.10 ± 0.09* |
| Ejection fraction (%) | 57.66 ± 2.37 | 63.11 ± 0.77 | 64.57 ± 0.61 | 57.55 ± 0.81* | 61.01 ± 0.66 | 54.34 ± 2.03* |
| Fractional shortening (%) | 34.94 ± 1.81 | 39.28 ± 0.64 | 40.49 ± 0.61 | 34.86 ± 0.62* | 37.56 ± 0.53 | 32.49 ± 1.48* |

LVEDD, left ventricle end diastolic diameter; LVESD, left ventricle end systolic diameter. Values are mean ± S.E.
$*P < 0.05$ *versus* control group.

TNF-α administration, and is dependent upon expression of inducible nitric oxide synthase and an increase in the levels of nitric oxide, which leads to sustained contractile dysfunction [32, 34]. In this study, we reported a novel finding of TNF-α-induced chronic myocardial dysfunction in mice that was characterized by ventricular dysfunctional changes on echocardiography in the presence of a slightly elevated antioxidant capacity in the plasma and total GSH levels in the ventricles. The molecular mechanism of TNF-α-induced chronic inflammation needs to be elucidated, but other published work and our unpublished observations suggest that pericardial and perivascular adipose tissue act as endocrine organs and sources of chronic inflammation [35, 36].

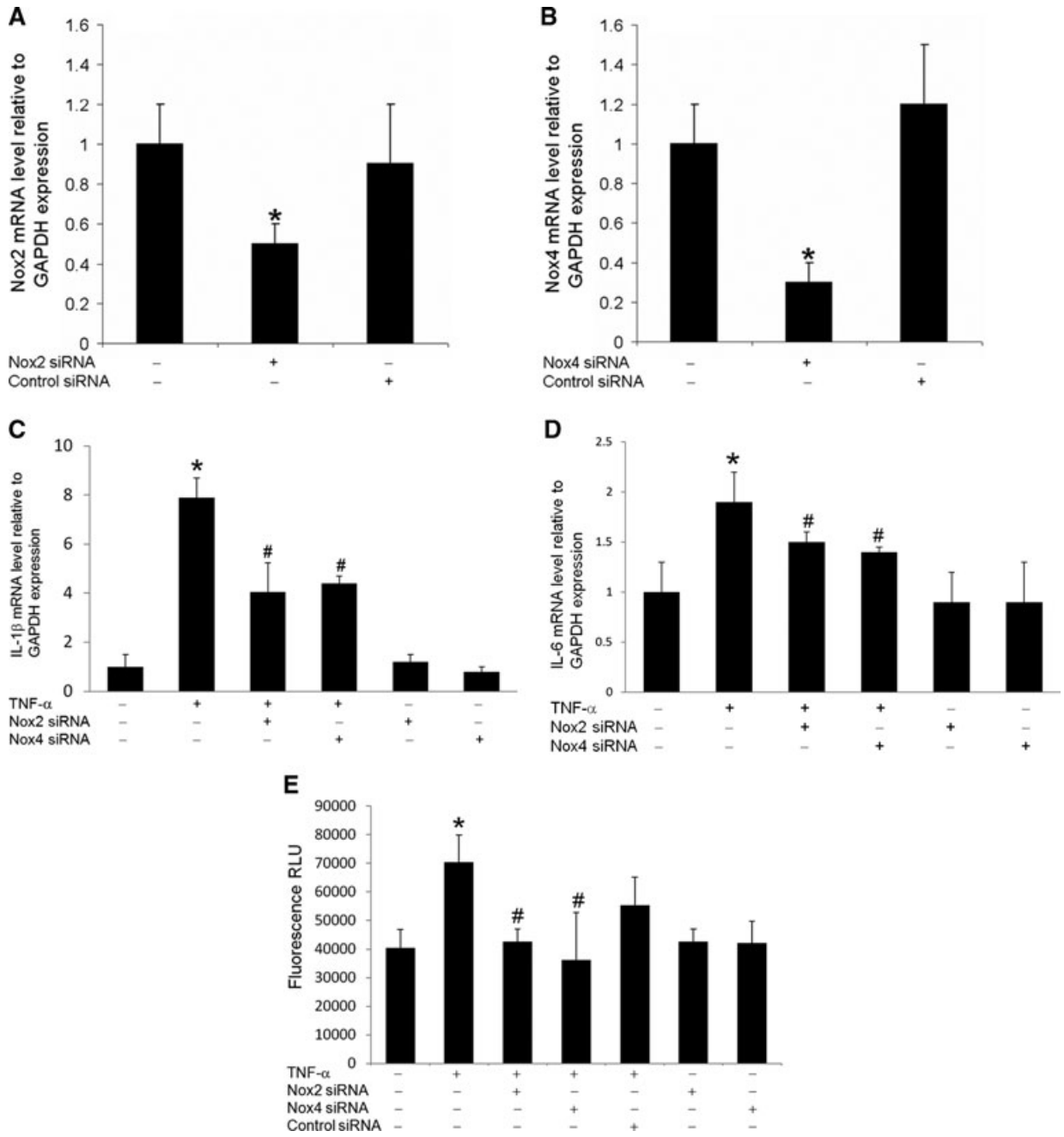


**Fig. 6** Nox2 and Nox4 mediate TNF-α-induced upregulation of IL-1β and IL-6 genes and ROS production. Human adult cardiomyocytes were transfected with Nox2 and Nox4 siRNA using siPORT Amine transfection reagents. Total RNA was extracted from human adult cardiomyocytes 24 hrs after transfection. Human Nox2 and Nox4 mRNA levels were examined using real-time PCR. Nox2 (**A**) and Nox4 (**B**) mRNA levels after siRNA treatment were shown. In the other experiments, cells were treated with TNF-α (20 ng/ml) for 6 hrs at 37°C after treatment with Nox2 and Nox4 siRNA. IL-1β (**C**) and IL-6 mRNA (**D**) levels were examined with real-time PCR. TNF-α-induced ROS production in human adult cardiomyocytes was determined with CM-$H_2$DCFDA following Nox2 and Nox4 siRNA treatment (**E**). Data were expressed as relative light unit (RLU) ± S.D. $^{*}P < 0.05$ *versus* control values. $^{\#}P < 0.05$ *versus* TNF-α treatment values.

Increasing evidence has shown that ROS induced by different stimuli are a cause of cardiac dysfunction and that NADPH oxidase plays a major part in ROS production [37]. This study demonstrated that an increase in the level of ROS in the ventricles was mediated by NADPH oxidase, but not by NOS, xanthine oxidase or mitochondrial respiration. Recently, Looi *et al*. [20] reported that the activity of NADPH oxidase was similar in a post-myocardial infarction cardiac remodelling model of wild-type and Nox2$^{-/-}$ mice, and suggested that the Nox 4 isoform could have a distinct role in the process. Moreover, another study confirmed that increased Nox4 at the mRNA and protein levels in the ventricles could compensate for Nox2 to increase the activity of NADPH oxidase in pressure-overload wild-type and Nox2$^{-/-}$ mice [13]. This study revealed that Nox2 and Nox4 had a crucial role by sequentially regulating TNF-α-induced ventricular remodelling in mice.

This study also showed that levels of IL-1β and IL-6 increased >100% from 1-day post-injection levels and were significantly higher than those in control mice. One study reported that elevated levels of TNF-α in infarcted myocardium contributed to acute myocardial rupture and chronic left ventricular dysfunction by inducing an excessive local inflammatory response [29]. Similarly, another study reported that an increase in the cardiac level of TNF-α after aortic banding for 2 weeks could be the source of an increase in pro-inflammatory cytokines, including IL-6, MCP-1 and MIP-1γ, in the ventricles of mice [18]. Moreover, TNF-α was reported to stimulate macrophages and other cell types to produce other pro-inflammatory cytokines, including IL-1, IL-6, IL-8 and TNF-α [38]. However, the molecular mechanism mediating generation of cytokines in the ventricles until 4 weeks after TNF-α treatment needs to be elucidated. It is possible that stressed myocardium, as indicated by increased ANP in our study, as well as skeletal muscle that was hypoperfused because of reduced cardiac output, could activate monocytes to produce cytokines which further lead to myocardial dysfunction [39]. The other possibility is that the heart acts as an endocrine organ and releases these cytokines [40]. This study convincingly showed that TNF-α-induced upregulation of IL-1β and IL-6 in human adult cardiomyocytes is mediated by Nox2 and Nox4, suggesting that NADPH oxidase has a crucial role in a cytokine-induced mechanism.

Our *in vitro* siRNA gene knockdown studies revealed that TNF-α-induced ROS production and upregulation of IL-1β and IL-6 in human adult cardiomyocytes are mediated by Nox2 and Nox4. We previously reported that TNF-α-induced ROS in human aortic smooth muscle cells was mediated by NADPH oxidase, specifically by Nox4, but not Nox2 [9]. Another report showed that TNF-α-induced activation of the transcription factors nuclear factor-kappa B (NF-κB) and stress-activated protein kinase/c-Jun N-terminal kinase led to the expression of several genes, including IL-1β, IL-6, platelet-derived growth factor, TGF-β and several other eicosanoids and hormones [41, 42]. A recent study reported that NADPH oxidases activate NF-κB, and suggested a potential role of NADPH oxidases in aging [43]. This study and unpublished work suggest that TNF-α-induced upregulation of IL-β and IL-6 *via* the NF-κB pathway is mediated by NADPH oxidase, inducing Nox2 and Nox4 subunits. However, one limitation of this study was that the *in vitro* studies could not simulate our *in vivo* findings because mimicking chronic inflammation in cell culture studies was not possible.

In summary, we described TNF-α-induced chronic ventricular remodelling in mice, characterized by ventricular inflammation, hypertrophied cardiomyocytes, ventricular dysfunction, and these effects were mediated by the sequential upregulation of Nox2 and Nox4. We also showed that NADPH oxidase plays a crucial role in TNF-α-induced ROS increase in this model. Finally, we identified a novel mechanism in which Nox2 and Nox4 mediate TNF-α-induced ROS, as well as upregulation of IL-1β and IL-6, in human adult cardiomyocytes.

## Acknowledgements

This work was funded by the National Medical Research Council and SingHealth Foundation, Singapore (awarded to K.T.M.).

## Conflict of interest

The authors confirm that there are no conflicts of interest.

## References

1. **Cohn JN, Ferrari R, Sharpe N.** Cardiac remodeling-concepts and clinical implications: a consensus paper from an international forum on cardiac remodeling. Behalf of an International Forum on Cardiac Remodeling. *J Am Coll Cardiol*. 2000; 35: 569–82.
2. **Paul S.** Ventricular remodeling. *Crit Care Nurs Clin North Am*. 2003; 15: 407–11.
3. **Torre-Amione G, Kapadia S, Benedict C, *et al.*** Proinflammatory cytokine levels in patients with depressed left ventricular ejection fraction: a report from the Studies of Left Ventricular Dysfunction (SOLVD). *J Am Coll Cardiol*. 1996; 27: 1201–6.
4. **Torre-Amione G, Kapadia S, Lee J, *et al.*** Tumor necrosis factor-alpha and tumor necrosis factor receptors in the failing human heart. *Circulation*. 1996; 93: 704–11.
5. **Bozkurt B, Kribbs SB, Clubb FJ Jr, *et al.*** Pathophysiologically relevant concentrations of tumor necrosis factor-alpha promote progressive left ventricular dysfunction and remodeling in rats. *Circulation*. 1998; 97: 1382–91.

6. **Kubota T, McTiernan CF, Frye CS, *et al.*** Cardiac-specific overexpression of tumor necrosis factor-alpha causes lethal myocarditis in transgenic mice. *J Card Fail*. 1997; 3: 117–24.
7. **Cave A, Grieve D, Johar S, *et al.*** NADPH oxidase-derived reactive oxygen species in cardiac pathophysiology. *Philos Trans R Soc Lond B Biol Sci*. 2005; 360: 2327–34.
8. **Lyle AN, Griendling KK.** Modulation of vascular smooth muscle signaling by reactive oxygen species. *Physiology (Bethesda)*. 2006; 21: 269–80.
9. **Moe KT, Aulia S, Jiang F, *et al.*** Differential upregulation of Nox homologues of NADPH oxidase by tumor necrosis factor-alpha in human aortic smooth muscle and embryonic kidney cells. *J Cell Mol Med*. 2006; 10: 231–9.
10. **Higashi M, Shimokawa H, Hattori T, *et al.*** Long-term inhibition of Rho-kinase suppresses angiotensin II-induced cardiovascular hypertrophy in rats *in vivo*: effect on endothelial NAD(P)H oxidase system. *Circ Res*. 2003; 93: 767–75.
11. **Sturrock A, Cahill B, Norman K, *et al.*** Transforming growth factor-beta1 induces Nox4 NAD(P)H oxidase and reactive oxygen species-dependent proliferation in human pulmonary artery smooth muscle cells. *Am J Physiol Lung Cell Mol Physiol*. 2006; 290: L661–73.
12. **Bendall JK, Cave AC, Heymes C, *et al.*** Pivotal role of a gp91(phox)-containing NADPH oxidase in angiotensin II-induced cardiac hypertrophy in mice. *Circulation*. 2002; 105: 293–6.
13. **Byrne JA, Grieve DJ, Bendall JK, *et al.*** Contrasting roles of NADPH oxidase isoforms in pressure-overload *versus* angiotensin II-induced cardiac hypertrophy. *Circ Res*. 2003; 93: 802–5.
14. **Zhao W, Zhao D, Yan R, *et al.*** Cardiac oxidative stress and remodeling following infarction: role of NADPH oxidase. *Cardiovasc Pathol*. 2009; 18: 156–66.
15. **Zhou Z, Kang X, Jiang Y, *et al.*** Preservation of hepatocyte nuclear factor-4alpha is associated with zinc protection against TNF-alpha hepatotoxicity in mice. *Exp Biol Med*. 2007; 232: 622–8.
16. **Weytjens C, Cosyns B, D'Hooge J, *et al.*** Doppler myocardial imaging in adult male rats: reference values and reproducibility of velocity and deformation parameters. *Eur J Echocardiogr*. 2006; 7: 411–7.
17. **Gigante B, Morlino G, Gentile MT, *et al.*** $Plgf^{-/-}eNos^{-/-}$ mice show defective angiogenesis associated with increased oxidative stress in response to tissue ischemia. *FASEB J*. 2006; 20: 970–2.
18. **Sun M, Chen M, Dawood F, *et al.*** Tumor necrosis factor-alpha mediates cardiac remodeling and ventricular dysfunction after pressure overload state. *Circulation*. 2007; 115: 1398–407.
19. **Maity P, Bindu S, Dey S, *et al.*** Indomethacin, a non-steroidal anti-inflammatory drug, develops gastropathy by inducing reactive oxygen species-mediated mitochondrial pathology and associated apoptosis in gastric mucosa: a novel role of mitochondrial aconitase oxidation. *J Biol Chem*. 2009; 284: 3058–68.
20. **Looi YH, Grieve DJ, Siva A, *et al.*** Involvement of Nox2 NADPH oxidase in adverse cardiac remodeling after myocardial infarction. *Hypertension*. 2008; 51: 319–25.
21. **Odaka C.** Localization of mesenchymal cells in adult mouse thymus: their abnormal distribution in mice with disorganization of thymic medullary epithelium. *J Histochem Cytochem*. 2009; 57: 373–82.
22. **Melgar S, Karlsson A, Michaelsson E.** Acute colitis induced by dextran sulfate sodium progresses to chronicity in C57BL/6 but not in BALB/c mice: correlation between symptoms and inflammation. *Am J Physiol Gastrointest Liver Physiol*. 2005; 288: G1328–38.
23. **Luyten CR, van Overveld FJ, De Backer LA, *et al.*** Antioxidant defence during cardiopulmonary bypass surgery. *Eur J Cardiothorac Surg*. 2005; 27: 611–6.
24. **Sherer TB, Betarbet R, Stout AK, *et al.*** An *in vitro* model of Parkinson's disease: linking mitochondrial impairment to altered alpha-synuclein metabolism and oxidative damage. *J Neurosci*. 2002; 22: 7006–15.
25. **Turan N, Csonka C, Csont T, *et al.*** The role of peroxynitrite in chemical preconditioning with 3-nitropropionic acid in rat hearts. *Cardiovasc Res*. 2006; 70: 384–90.
26. **Mukhopadhyay P, Rajesh M, Batkai S, *et al.*** Role of superoxide, nitric oxide, and peroxynitrite in doxorubicin-induced cell death *in vivo* and *in vitro*. *Am J Physiol Heart Circ Physiol*. 2009; 296: H1466–83.
27. **Gertzberg N, Neumann P, Rizzo V, *et al.*** NAD(P)H oxidase mediates the endothelial barrier dysfunction induced by TNF-alpha. *Am J Physiol Lung Cell Mol Physiol*. 2004; 286: L37–48.
28. **Moe TK, Ziliang J, Barathi A, *et al.*** Differential expression of glyceraldehyde-3-phosphate dehydrogenase (GAPDH), beta actin and hypoxanthine phosphoribosyltransferase (HPRT) in postnatal rabbit sclera. *Curr Eye Res*. 2001; 23: 44–50.
29. **Sun M, Dawood F, Wen WH, *et al.*** Excessive tumor necrosis factor activation after infarction contributes to susceptibility of myocardial rupture and left ventricular dysfunction. *Circulation*. 2004; 110: 3221–8.
30. **Levine B, Kalman J, Mayer L, *et al.*** Elevated circulating levels of tumor necrosis factor in severe chronic heart failure. *N Engl J Med*. 1990; 323: 236–41.
31. **Kuntz ID, Chen K, Sharp KA, *et al.*** The maximal affinity of ligands. *Proc Natl Acad Sci USA*. 1999; 96: 9997–10002.
32. **Meldrum DR.** Tumor necrosis factor in the heart. *Am J Physiol*. 1998; 274: R577–95.
33. **Oral H, Dorn GW 2nd, Mann DL.** Sphingosine mediates the immediate negative inotropic effects of tumor necrosis factor-alpha in the adult mammalian cardiac myocyte. *J Biol Chem*. 1997; 272: 4836–42.
34. **Nussler AK, Billiar TR.** Inflammation, immunoregulation, and inducible nitric oxide synthase. *J Leukoc Biol*. 1993; 54: 171–8.
35. **Kershaw EE, Flier JS.** Adipose tissue as an endocrine organ. *J Clin Endocrinol Metab*. 2004; 89: 2548–56.
36. **Berg AH, Scherer PE.** Adipose tissue, inflammation, and cardiovascular disease. *Circ Res*. 2005; 96: 939–49.
37. **Hamilton CA, Miller WH, Al-Benna S, *et al.*** Strategies to reduce oxidative stress in cardiovascular disease. *Clin Sci*. 2004; 106: 219–34.
38. **Mann DL, Young JB.** Basic mechanisms in congestive heart failure. Recognizing the role of proinflammatory cytokines. *Chest*. 1994; 105: 897–904.
39. **Seta Y, Shan K, Bozkurt B, *et al.*** Basic mechanisms in heart failure: the cytokine hypothesis. *J Card Fail*. 1996; 2: 243–9.
40. **Stephenson TJ, Broughton Pipkin F.** Atrial natriuretic factor: the heart as an endocrine organ. *Arch Dis Child*. 1990; 65: 1293–4.
41. **Feldman AM, Combes A, Wagner D, *et al.*** The role of tumor necrosis factor in the pathophysiology of heart failure. *J Am Coll Cardiol*. 2000; 35: 537–44.
42. **Nian M, Lee P, Khaper N, *et al.*** Inflammatory cytokines and postmyocardial infarction remodeling. *Circ Res*. 2004; 94: 1543–53.
43. **Clark RA, Valente AJ.** Nuclear factor kappa B activation by NADPH oxidases. *Mech Ageing Dev*. 2004; 125: 799–810.